



HAL
open science

Antimycotic effects of the plasma gun on the yeast *Candida glabrata* tested on various surfaces

Kristína Trebulová, Inna Orel, Jean-michel Pouvesle, Eric Robert, Amaury Rouillard, Augusto Stancampiano, Jan Hrudka, Přemysl Menčík, Zdenka Kozáková, Zuzana Měšťánková, et al.

► To cite this version:

Kristína Trebulová, Inna Orel, Jean-michel Pouvesle, Eric Robert, Amaury Rouillard, et al.. Antimycotic effects of the plasma gun on the yeast *Candida glabrata* tested on various surfaces. *Plasma Processes and Polymers*, In press, 10.1002/ppap.202400057 . hal-04660548

HAL Id: hal-04660548


<https://hal.science/hal-04660548v1>

Submitted on 24 Jul 2024

HAL is a multi-disciplinary open access archive for the deposit and dissemination of scientific research documents, whether they are published or not. The documents may come from teaching and research institutions in France or abroad, or from public or private research centers.

L'archive ouverte pluridisciplinaire **HAL**, est destinée au dépôt et à la diffusion de documents scientifiques de niveau recherche, publiés ou non, émanant des établissements d'enseignement et de recherche français ou étrangers, des laboratoires publics ou privés.

Antimycotic effects of the plasma gun on the yeast *Candida glabrata* tested on various surfaces

Kristína Trebulová¹  | Inna Orel² | Jean-Michel Pouvesle² | Eric Robert² | Amaury Rouillard² | Augusto Stancampiano² | Jan Hrudka³ | Přemysl Menčík¹ | Zdenka Kozáková¹ | Zuzana Měšťánková¹ | Darina Kužmová¹ | Ivana Paličková⁴ | Alois Čížek⁴ | František Krčma¹

¹Faculty of Chemistry, Brno University of Technology, Brno, Czech Republic

²GREMI, UMR7344 CNRS/University of Orleans, Orléans, France

³Faculty of Chemical Engineering, University of Chemistry and Technology Prague, Praha, Czech Republic

⁴Faculty of Veterinary Medicine, University of Veterinary Sciences Brno, Brno, Czech Republic

Correspondence

Kristína Trebulová, Faculty of Chemistry, Brno University of Technology, Purkyňova 118, 612 00 Brno, Czech Republic.
Email: trebulovakristina@gmail.com

Funding information

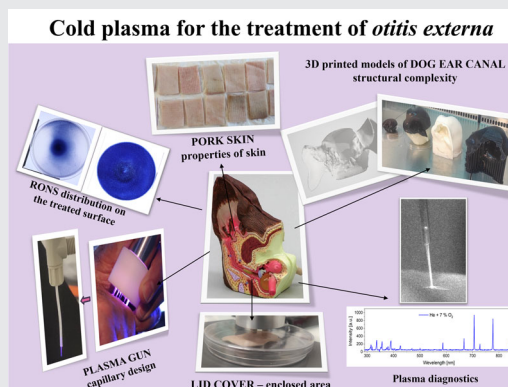
COST Action CA20114; COST Action CA19110; GDR HAPPYBIO

Abstract

This work focuses on the antimycotic effects of the plasma gun as a potential tool for the treatment of superficial infections. *Candida glabrata* was chosen as a model microorganism. The preliminary tests have been done on the agar plates to establish the basic plasma parameters. To render this research more appropriate to the real application, more complex inoculation substrates, pork skin and 3D-printed models of the dog ear canal have been used. The results of this work confirm the high efficiency of cold plasma in the inhibition of yeasts on different surfaces and will lead to further experiments.

KEYWORDS

antimicrobial effects, cold plasma, *otitis externa*, plasma medicine



1 | INTRODUCTION

Cold atmospheric-pressure plasma (CAP) technology has become a very discussed topic in the past three decades, thanks to its wide range of applications in various fields of industry and biomedicine. With the

ever-increasing resistance of microbes against antimicrobials,^[1] there arises an urge to find alternative treatments for many diseases not only in the human world but also in the animal and plant kingdoms. This study focuses on the animal kingdom and veterinary application of CAP. One of the diseases that deserves

Abbreviations: *C. glabrata*, *Candida glabrata*; CAP, cold atmospheric-pressure plasma; RNS, reactive nitrogen species; RONS, reactive oxygen and nitrogen species; ROS, reactive oxygen species.

special attention is *otitis externa* (inflammation of the ear canal) in dogs.

1.1 | Otitis externa

Otitis externa, or so-called swimmer's ear, is a condition that causes inflammation of the external ear canal, which is the tube between the outer ear and the eardrum.^[2] In dogs, the prevalence of this disease is in the range of 5%–20%, depending on the dog's race and predispositions as well as on the external climate conditions.^[3] When selecting therapy, it is important to bear in mind that this is a multifactorial disease and therefore, the medication is never one-sided. Solutions combining active substances with both antibacterial and antifungal activity while adding corticosteroids and other nonsteroid anti-inflammatory substances are recommended to relieve swelling, itching and redness. Other substances, including surfactants, cerumenolytic agents and astringents, are also involved in rendering the treatment successful.^[4] These medications are usually prescribed in a typical form, such as ear drops, solutions, or emulsions.^[5,6] Selection of antibiotics for the treatment can be problematic due to the resistance of the microbes to many classes of antimicrobials, and the treatment is further complicated by the increasing number of multidrug-resistant strains. If the inflammation stays untreated or with improper treatment, otitis externa can progress to a chronic stage, which can lead to eardrum rupture, otitis media and, in extreme cases, deafness.^[7,8] Improper use of antibiotics can also lead to the development of microbial resistance to the antimicrobials used.^[5,9]

Otitis externa is usually caused by either bacteria (*Staphylococcus pseudintermedius*, *Pseudomonas aeruginosa*) or yeasts (*Malassezia pachydermatis* and *Candida* species).^[10] As a model microorganism, the yeast *Candida glabrata* was chosen due to its more complex cellular structure compared to the bacterial cells.

1.1.1 | CAP

CAP operates at room temperature and atmospheric pressure, making it a unique and highly versatile technology. Unlike traditional plasmas that require high temperatures or low pressures, CAP offers several advantages for various applications, ranging from surface treatment and decontamination to medicine and agriculture. CAP produces a wide range of reactive particles, including electrically charged particles, such as ions and electrons, as well as excited neutral species.^[11] These

species have energy high enough to react with other species or objects, while heavier particles of neutral gases have lower kinetic energy, providing lower thermal heating. The CAP also induces an electromagnetic field and a production of photons, some of which are in the UV and even VUV regions. This unique combination of properties allows CAP to interact with a wide range of materials, surfaces, and biological systems while minimizing thermal damage.^[12,13]

CAP can be generated using different plasma systems from which one group is composed of various atmospheric-pressure plasma jets. The plasma jets generate nonthermal plasmas that can operate at atmospheric pressure, making them highly suitable for numerous industrial and scientific applications. By utilising a range of feed gases and applying high-voltage electrical discharges, atmospheric-pressure plasma jets produce a flux of highly reactive charged particles, radicals, and photons, as well as induce the electromagnetic field.^[14,15]

Plasma jets produce discharges that can propagate outside the plasma reactor, thus allowing the treatment of virtually any surface independently of the target nature, size, or morphology. Thus, the use of plasma jets can be accommodated to a specific target or application.^[16]

For a specific application—the treatment of an irregular cavity such as the dog's external ear canal—the plasma gun with its capillary design^[17] was selected for this study.

2 | MATERIALS AND METHODS

2.1 | Plasma gun

The plasma gun developed at GREMI is based on a dielectric barrier discharge across a glass capillary ($\varnothing_{\text{outer}} = 6$ mm and $\varnothing_{\text{inner}} = 4$ mm) equipped with an inner hollow high-voltage electrode and an external grounded ring electrode.^[17] This set-up will be referred to as the big capillary (BC). In this work, high purity (99.999%) helium (2.2 L/min) and helium with oxygen admixtures (0.5% and 0.7% corresponding to 10 and 15 mL/min as mentioned in Table 1) were used as a feed gas with the flow rate set and controlled with the Red-y Vögtlin instruments flowmeters. The DBD discharge was powered with a Gaussian-shaped high-voltage pulse having a full width at half maximum of $2 \mu\text{s}$, the peak voltage amplitude was 4 kV, and the pulse repetition rate was 8 kHz. An 8 cm long silicone capillary ($\varnothing_{\text{outer}} = 2$ mm and $\varnothing_{\text{inner}} = 1$ mm) was plugged through a dielectric connector at the outlet of the baseline glass capillary. To allow the CAP operation at low voltages, high voltage was delivered via a

TABLE 1 Experimental set-up parameters.

Voltage amplitude (kV)	4		
Average power delivered to the target (W)	<1		
Operating frequency (kHz)	8		
Distance of the capillary ending from the treated surface (mm)	1	6	10
Treatment time (min)	0.5–15		
Carrier gas (helium) (L/min)	2.2		
Oxygen admixture (mL/min)	0	10	15
Plasma capillary size (mm)	Big capillary: $\varnothing_o = 6$; $\varnothing_i = 4$	Small capillary: $\varnothing_o = 2$; $\varnothing_i = 1$	

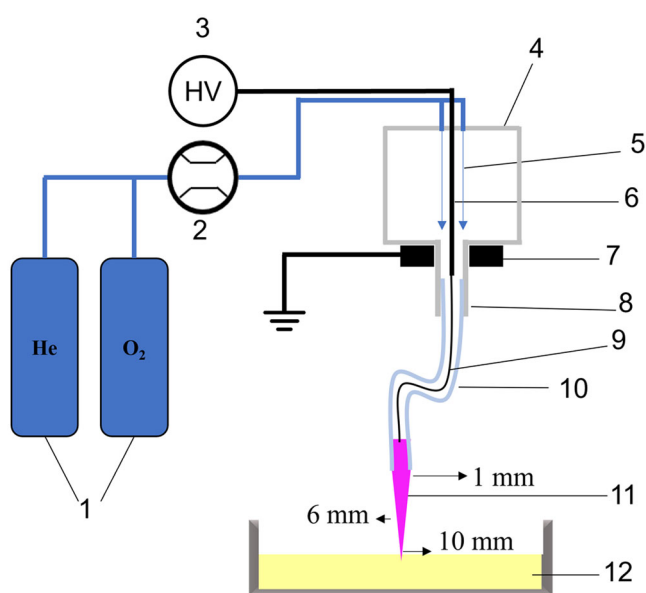


FIGURE 1 Scheme of the plasma gun and the treatment set-up; 1—gas bottles, 2—gas flowmeter, 3—high-voltage power supply, 4—dielectric reactor case, 5—gas flow, 6—high-voltage electrode, 7—ground electrode, 8—glass capillary (later referred as big capillary [BC]), 9—flexible HV electrode extension, 10—extended thinner silicone capillary (later referred as small capillary [SC]), 11—plasma plume, and 12—inoculated Petri dish.

thin (300 μm in diameter) wire electrode that ended 1 cm before the outlet of the small diameter capillary. This plasma set-up will be later referred to as the small capillary (SC). Plasma treatment was also performed with the original design of the plasma gun (the BC). In this latter configuration, the thin wire was not used, and the inner powered electrode tip was also set 1 cm before the outlet of the glass capillary. The plasma set-up can be seen in Figure 1.

The microsecond pulse waveform allows controlled plasma propagation in high aspect ratio capillaries, likely to be used for endoscopic plasma treatment.^[18]

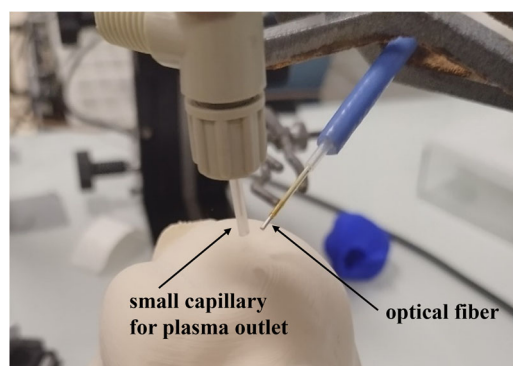


FIGURE 2 Optical emission spectrometry set-up for the recording of emission spectra from the plasma plume.

2.2 | Optical emission spectrometry (OES)

The light emitted by the plasma plume was collected through a quartz optical fibre (Figure 2) and analysed by means of a spectrometer (Oceanoptics Maya Pro 2000). The spectra were averaged over 12 acquisitions of 500 ms of exposure each.

2.3 | Microbiology

For the testing of the antimicrobial activity, the yeast strain *C. glabrata* CCM 8270 supplied by the Czech Collection of Microorganisms in Brno^[9] was used. The yeast inoculum was prepared to the YPD (Yeast extract—Peptone—Dextrose/Glucose) liquid medium and cultivated in the thermoregulated shaker at the temperature of 37°C for 24 h. The cultivation temperature was chosen as the standardly used temperature for the cultivation of mesophilic microorganisms. It is the temperature that corresponds to a normal human body temperature,

where *C. glabrata* can grow and cause candidiasis. In the dog ear canal, where the *otitis externa* develops, the temperature varies from 37°C to 40°C in resting conditions.^[19] To make the results comparable with results achieved for different microbial cultures in different experiments the temperature 37°C was chosen.

For all experiments (agar-plate based, pork skin and dog ears models), three biological replicates with two technical replicates for each biological replicate were performed.

The experiments were performed in a way to avoid the temperature rise of the treated surface and not to exceed the temperature tolerance of the human skin.^[20–22] Temperature measurements of the target surface were done by means of an infrared camera (FLIR E5). The data confirmed that the surface temperature did not exceed 40°C during the operation of the plasma reactor on any of the tested inoculation materials (agar plates, pork skin, and dog ear models).

2.3.1 | Sample preparation, plasma treatment and evaluation methods

Agar plate-based experiments

Sterile YPD medium was poured evenly into plastic Petri dishes with a diameter of 90 mm so that the agar layer was about 2 mm thick. The 24-h inoculum of *C. glabrata* was diluted to an approximate concentration of 10⁶ CFU/mL and inoculated on the agar plates to form a confluent layer on the agar surface.

C. glabrata cultures were exposed to the plasma immediately after the inoculation. Each Petri dish was treated individually, with the plasma plume oriented perpendicularly to the sample and approx. to the centre of the Petri dish. Two different capillary sizes were tested at the constant gas flow. The diameters of the capillaries were following (a) the original plasma gun set-up referred as the BC with the inner diameter (\varnothing_i) equal to 4 mm and the outer diameter (\varnothing_o) of 6 mm; (b) the thin capillary more convenient for the chosen veterinary application referred as the SC with the inner diameter (\varnothing_i) of 1 mm and the outer diameter (\varnothing_o) of 2 mm.

Different settings of the plasma set-up were tested (see Table 1). A lid from a Petri dish with a hole inside (the size of the corresponding capillary) was used to cover a series of the treated samples. Inoculated, nontreated Petri dishes were left as control samples for each experiment.

The treated samples were subsequently cultivated in an incubator (37°C). The temperature of 37°C was selected as an optimal growth temperature standardly used for the cultivation of mesophilic microorganisms. All Petri dishes were photographed 24, 48 and 72 h after

the plasma treatment. The inhibited surface area was quantitatively assessed in collaboration with HexTech Research s.r.o. using the Aurora software.^[23] The Aurora programme employs advanced artificial intelligence techniques, specifically machine learning algorithms, to categorise pixels based on their spectral intensities. Consequently, it can differentiate between the agar, ambient environment and the microbial culture, as depicted in Figure 3. The software outputs the proportion of the area occupied by the microbial culture. To determine inhibition efficiency, the area percentage of the yeast in the treated sample is subtracted from that of the control samples. Then, it is possible to estimate the inhibition efficiency as the decontamination capacity of the CAP per the treated area (64 cm²). Results were also statistically evaluated using the software Statistica. Standard statistical tools were used to evaluate the significance of achieved results. According to the data characteristics, appropriate tests were chosen to calculate the value of significance (*p*-value) with a significance level $\alpha = 0.5$.

Pork skin

A flat piece of fresh pork skin was bought in a conventional grocery store, and the remaining meat was removed, but the fat layer was preserved. The pork skin was cut into small pieces (3 × 4 cm²) and washed in soapy water to remove any remaining blood

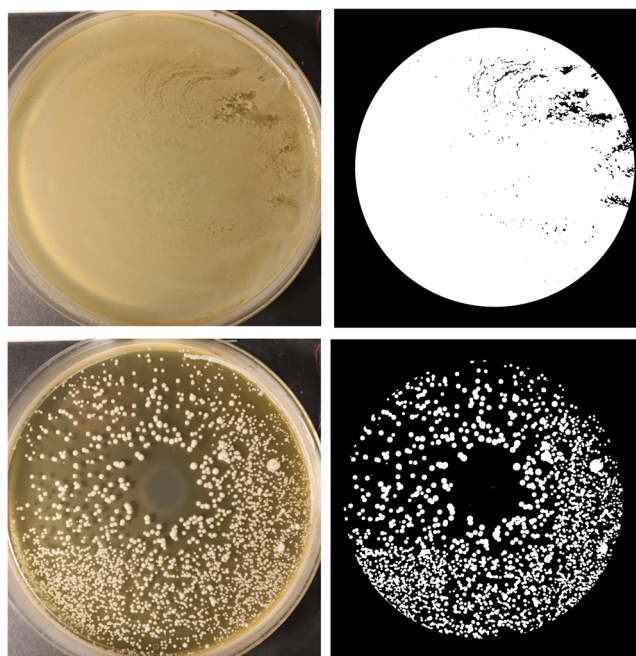


FIGURE 3 Demonstration of the evaluation method using the software Aurora; control sample (top), treated sample (bottom).

and dirt from the surface. After washing, the skin pieces were dried using a special filtration paper and put into an ethanol (70%) shaking bath for 15 min. Afterwards, the pieces were dried again and laid into the Petri dishes so that each piece was separated from the others. Then, these samples were put under the UV lamp of the biosafety cabinet (ThermoScientific MSC-Advantage, class II, UVC 254 nm) and irradiated for 10 min from both sides. After this procedure, the skin pieces were ready to be used as an inoculation substrate.

After the decontamination procedure, each pork skin was inoculated with 10, 20 or 50 μL of the fresh undiluted 24-h inoculum of *C. glabrata* (its preparation is mentioned above). Each droplet of microbial culture was put on the top skin layer (*stratum corneum*) and spread with a cell spreader over the whole surface area of the skin piece. Immediately after the inoculation, the skin pieces were exposed to the plasma.

Each piece was treated individually, with the plasma plume oriented perpendicularly to the sample surface, approximately to the centre of the skin piece. Two different capillary sizes (BC and SC) were tested at the constant gas flow ($Q_{\text{He}} = 2.2 \text{ l/min}$; $Q_{\text{O}_2} = 15 \text{ mL/min}$), high voltage ($U = 4 \text{ kV}$) and operating frequency ($\nu = 8 \text{ kHz}$). Experiments in pure helium as the plasma gas were performed in the same manner. Chosen treatment times were 3, 5 and 15 min for conditions with and without the lid from the Petri dish. The distance from the capillary ending to the surface of the pork skin was approximately 6–10 mm so that the tip of the plasma plume would directly touch the treated surface. All measurements were replicated twice, and control samples without the plasma treatment, as well as controls for pork skin sterility, were evaluated.

The treated samples were subsequently cultivated in the thermostat (37°C) for 24 h. After the 24 h incubation, the pork skin pieces were washed with sterile water (3 mL each piece). Then, this water was used for the inoculation and evaluation via the standard plate count method. Dilution rows (four 10-fold dilutions) were prepared, and 10 μL droplets were inoculated onto the semi-solid agar plates (their preparation mentioned above).^[24] Each dilution was inoculated four times (replicates of four droplets in a row). All the agar plates were cultivated in the thermostat (37°C) and photographed after 24, 48 and 72 h. The colonies in each droplet were counted and turned into CFU/mL. The measurements of optical density in the 96-microwell plates were also performed. Undiluted wash water (150 μL) was pipetted into 96-microwell plates, and sterile YPD medium

(100 μL) was added into each well. The 96-microwell plates were measured immediately and then 24, 48 h and 5 days after the treatment, meanwhile stored in the thermostat (37°C).

3D-printed models of dog ears

A model of a dog head was downloaded from a freely accessible online database of 3D models.^[25] The model was acquired using computed tomography (CT) and considers the internal structure of the dog's auditory system, including the external overhanging auricles. The model was further modified in the PrusaSlicer software so that the pinnae were removed from the model to allow access into the inner ear system. PrusaSlicer is based on an open-source platform called Slic3r, licensed under the GNU Affero General Public License. Then, this adapted model of the dog head with two ear canals (one from each side) was prepared for printing on the Original Prusa i3 MK3S + 3D printer (by Prusa Research a.s. in Prague, Czech Republic) and using the Fused Deposition Modelling (FDM) printing method. For all the printings, the nozzle with a diameter of 0.4 mm was used, and the layer height was 0.2 mm. Polylactide (PLA) was selected as a printing material due to its nontoxic nature and easy printing conditions. Three sizes of dog heads were chosen (large, medium and small) to represent the various sizes of the dogs (see Figure 4). The 3D-printed models were decontaminated using ethanol (70%) wash and UV radiation inside the laminar flow hood for 60 min (preset by the flow hood settings). After this decontamination procedure, the models were ready for inoculation.

The 24-h inoculum of *C. glabrata* (preparation mentioned above) was diluted to approx. concentration of 10^5 CFU/mL into the liquid YPD medium. Different sizes of the 3D-printed models were inoculated with different volumes of the microbial culture (see Table 2). After the inoculation, a 15-min break was established for the cells to adhere to the surface. Subsequently, each dog ear canal was treated for 15 min by the plasma gun: (a) either on the surface only (scanning the surface using a hand motion and holding for ~ 2 min at each chosen 5 mm^2 spot), (b) inside the cavity, only (scanning the different parts of the cavity and holding for ~ 2 min at each chosen spot), or (c) total treatment of the surface and the cavity (continuous scanning of the whole ear and the cavity holding at each chosen spot for approx. 1 min). Only the SC was used for these experiments with the constant gas flow ($Q_{\text{He}} = 2.2 \text{ l/min}$; $Q_{\text{O}_2} = 15 \text{ mL/min}$), at fixed voltage, and operating frequency ($U = 4 \text{ kV}$, $\nu = 8 \text{ kHz}$). Experiments with only helium as the plasma gas were performed with the other parameters unchanged. For each dog head, one ear canal was

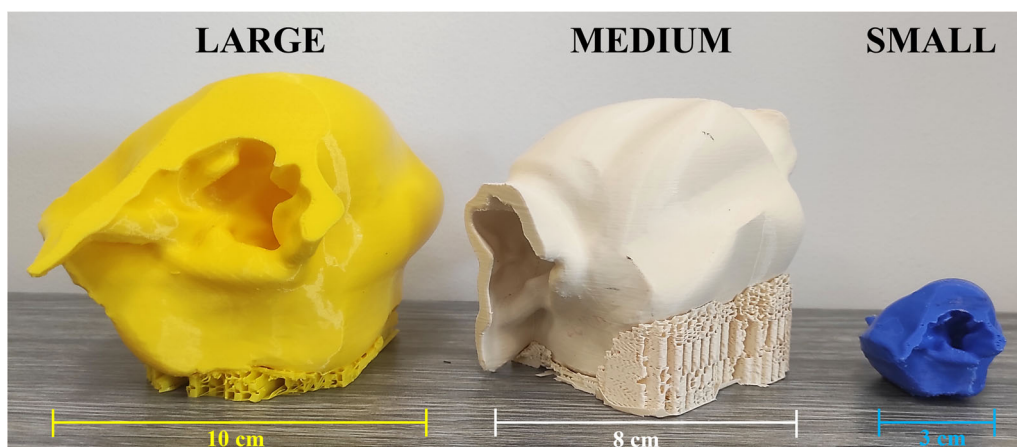


FIGURE 4 3D-printed models of the dog ear in various sizes.

TABLE 2 Dog ear canal treatment set-up.

Dog ear model	Inoculation volume (mL)	Wash water volume (mL)
Small	0.2	1
Medium	1	5
Large	2	5

used for the treatment, and the other was left as a control sample. Three samples were treated for each dog head size. Controls of the sterility of the 3D models before inoculation were performed as well.

After the treatment, the ear canal was washed with sterile water (different volumes for different ear sizes—see Table 2). Then, the content of the ear canal (wash water and the treated microbial culture) was poured into a sterile Petri dish and used for three different evaluation techniques. First, the inoculation was done using the dilution row (four 10-fold dilutions), where 10 μ L droplets were inoculated onto the solid agar plates (preparation mentioned above). Second, the undiluted content (150 μ L) was pipetted into 96-microwell plates, and sterile liquid YPD medium (100 μ L) was added to each well. The 96-microwell plates were measured immediately after the treatment, as well as 24 and 48 h after the treatment, meanwhile stored in the thermostat (37°C). Lastly, the remaining sample was poured onto the solid agar plates and left to settle for 10 min in a flow hood at room temperature. Then, the remaining water was pipetted out from the Petri dishes. All agar plates were cultivated in the thermostat (37°C) and photographed after 24, 48 and 72 h. The “inundated” Petri dishes were evaluated in cooperation with the HexTech Research s.r.o. using the software Aurora.^[23] In the

case of the dilution rows, the number of colonies was counted.

2.3.2 | Preparation and treatment of agar-based biopolymer with potassium iodide (KI)

The KI-enriched biopolymers were prepared to prove the presence of ROS and to monitor their distribution. The mixture was prepared using 2.2 g of agar, 100 mL of distilled water, 0.5 g of KI and 0.4 g of corn starch and heated with constant stirring until the boiling point temperature. When the boiling temperature was reached, the hot mixture was poured into Petri dishes with a diameter of 90 mm (10 mL into each dish). After the solidification of the mixture by its cooling, the KI-enriched biopolymers were ready for the plasma treatment.

Most of the plasma set-up conditions used for the proof reactions were the same as in the experiments with the pork skin: two capillary sizes, changing the amount of oxygen in the gas flow (0%, 0.50.5% and 0.7%). Treatment times were 5 and 15 min with and without the lid. All the KI-enriched biopolymers were photographed directly after the treatment.

2.3.3 | Testing of the *C. glabrata* antimycotic resistance

The 24-h inoculum of *C. glabrata* was diluted (approx. concentration of 10⁶ CFU/mL), inoculated on the solid agar plates and spread evenly on the surface to form a homogenous layer. Antimycotic discs (ITEST plus s.r.o.) containing the antimycotics in selected concentrations were placed on the agar plates in a star-like manner (shown later in the text in Figure 11). Then, these plates were stored in the thermostat (37°C) and evaluated after 24 h. Evaluation

was done by measuring the sizes of the inhibition zones and comparing them with the values in the tables for antimicrobial resistance provided by the disc supplier.

3 | RESULTS

3.1 | OES

Figure 5 reports the spectra obtained for the cases on the dog model for different concentrations of oxygen in the working gas. The case with only He in the feed gas represents the spectra characteristic of a cold plasma jet dominated by the nitrogen second positive system emission (300–450 nm), and He lines (i.e., 587 and 706.5 nm). With increasing oxygen concentration in the feed gas, there is a decrease of the emission associated with nitrogen second positive system and an increase of emission associated with atomic oxygen at 77 nm. A higher concentration of atomic oxygen is associated with a higher concentration of ROS and may lead, as observed, to higher inactivation potential. The same trends were observed for the agar and pork skin substrates (not shown).

3.2 | Optimisation of the plasma treatment

The optimisation of the plasma treatment was based on the previous experiments with bacteria *Escherichia coli* and *Staphylococcus aureus*,^[26,27] where, different voltages, treatment times, gas compositions and the treatment distance were chosen for sufficient bacterial inhibition. Based on this work, similar plasma set-ups were tested and modified for successful yeast inhibition. These experiments were done on the Petri dishes and a detailed description of the experimental set-up was mentioned above.

3.2.1 | Agar plate-based experiments

All the measurements were done for the small and the BC, respectively.

Input voltage, treatment time and treatment distance
For the small and the BC, it was proven that higher inhibition efficiency can be achieved with higher input voltage and longer treatment time, as expected according

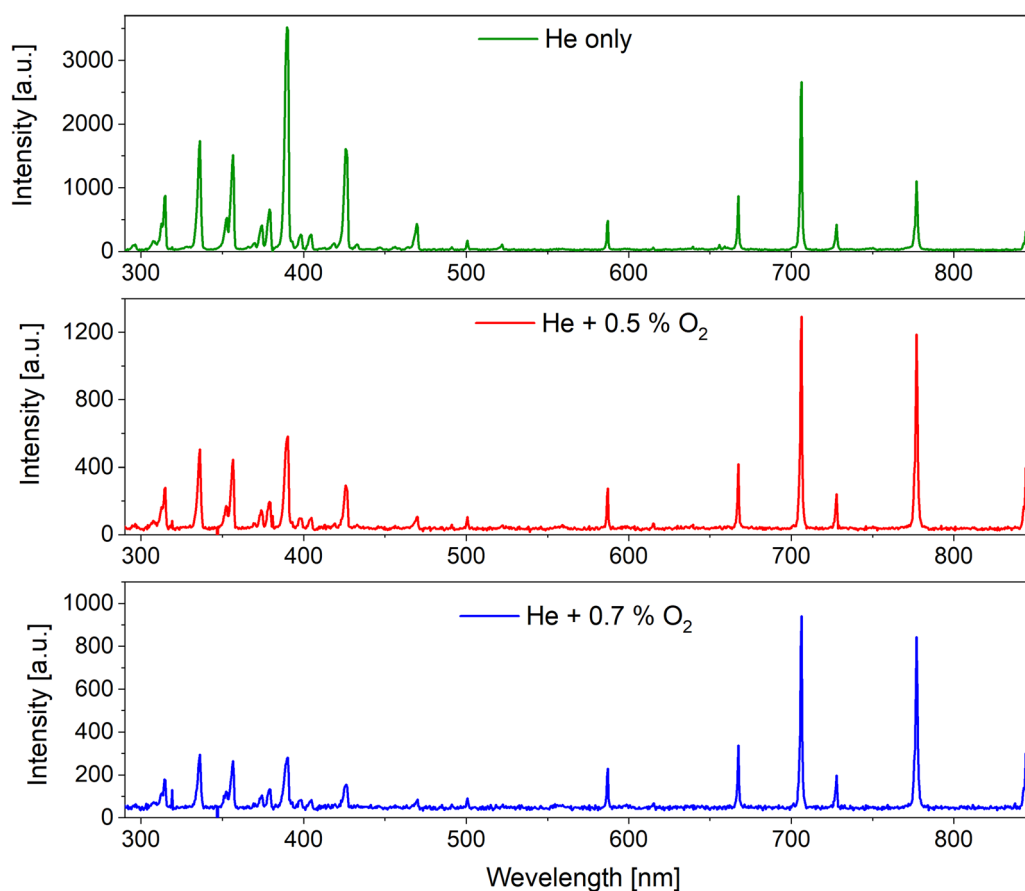


FIGURE 5 Emission spectra from the plasma plume in contact with one of the dog models for different concentrations of oxygen in the feed gas.

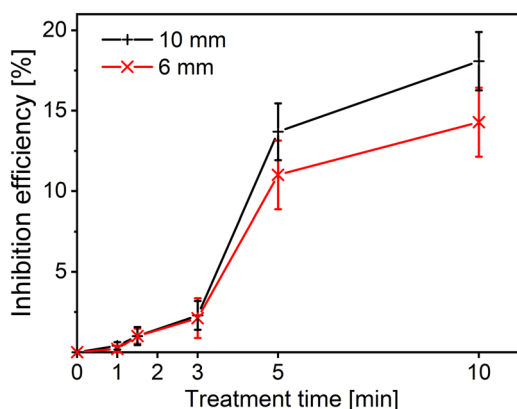


FIGURE 6 Dependence of the inhibition efficiency on the treatment time for two distances between the end of the capillary and the treated surface, big capillary ($\varnothing_i = 4$ mm); input voltage of 4 kV. Note: results for the distance 1 mm are not reported because the inhibition efficiency was negligible.

to the previous experiments.^[16,26,28] Compared to the bacterial experiments, the treatment time had to be extended from 30–60 s (bacteria) to 10–15 min (yeast) to achieve similar inhibition efficiency. As can be seen in Figure 6, the inhibitory effects of the open-air treatment are negligible with the short treatment times and start to be remarkable after the 5-min treatment. From that treatment time, the inhibition efficiency slightly increases with further treatment duration. In the plasma jets, most active particles are located at the boundary of the plasma plume with the ambient air, where efficient energy transfers from the helium or helium-based plasma occur with air constituting molecules (oxygen, nitrogen and water vapour). Such energy transfers lead to so-called RONS generation, mostly at the interface between the plasma plume and ambient air. The RONS concentration exhibits a strong gradient from this interface to the outermost distances from the plasma plume. Nevertheless, longer treatment time will gradually result in the accumulation and diffusion of long-lived RONS at larger distances from the plasma plume contact zone on the sample. It is expected that if RONS concentration gradually overpasses the threshold for microbial inactivation, the longer treatment time will result in the extension of the inhibition area.^[29] Much larger inhibition efficiency could be achieved if the plasma plume was scanning the treated surface.

Three different distances of the capillary ending from the agar surface (1, 6 and 10 mm) were chosen to optimise the treatment distance. The top of the plasma plume was touching the treated surface (1 mm), and the middle part of the plasma plume was in contact with the treated surface (6 mm), as shown in Figure 1. The case where only the tip of the plasma plume was directly

touching the agar surface (10 mm) came out to be the most efficient (see Figure 6). Similar trends were observed in other plasma sources as well.^[30] However, if we increased the distance even more and there would be no contact between plasma and the treated surface, the efficiency of the treatment would decrease rapidly as the short-lived species would react or recombine before getting to the target. In our experimental conditions, the highest inhibition efficiency is achieved for the gap distance large enough to favour RONS generation at the boundary of the plasma plume with ambient air while keeping the plasma plume in contact with the treated sample. This tends to indicate that the combined action of long and short-living RONS is the more efficient protocol for yeast decontamination. Although from the statistical point of view, the treatment distance does not appear significant ($p = 0.048$), it is important to strive for better efficiency when possible. That is why from this optimisation step, the following treatments were adjusted in a way that the tip of the plasma plume touched the surface.

Concept of covering the treated surface

An endoscopic treatment in the closed space was tested to mimic the treatment inside the dog's ear canal. In experiments held on the Petri dishes, the closed space was simulated using the lid from the Petri dish with a small hole in the size of the capillary (i.e., a different lid was used for the small and the big capillaries). The usage of the lid to cover the treated surface resulted in a tremendous enhancement of the inhibition efficiency (see Figure 7). The significant difference between the results with and without the lid is also supported from the statistical standpoint ($p = 0.028$). In the open-air treatment, the inhibition efficiency after the 15-min treatment was up to 20%, whereas with the usage of the lid, it was possible to decontaminate almost 80% of the treated area. The inhibitory effects were not only visible in the form of a compact circular zone without any microbial growth but a decreased microbial growth was also observed spreading outwards through the whole treated surface. By covering the treated surface with the lid, we drastically reduce the dissipation of the RONS into the open air. When the RONS are entrapped under the lid, the long-lived species can be accumulated and distributed over the covered area, which provides better inhibition efficiency. It was proved that the prevalent long-lived species formed in the plasma gun are ozone molecules, which are well known for their antibacterial properties.^[31] So, the reason behind the enhanced decontamination lies in the accumulation of RONS (probably mainly ozone) under the lid, where they react with the treated surface. This concept of covering the

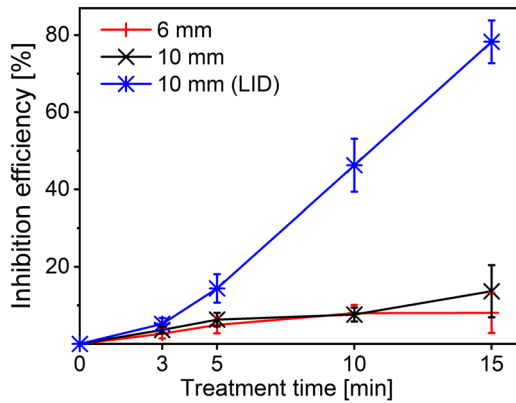


FIGURE 7 Dependence of the inhibition efficiency on the treatment time for two distances in the open-air treatment and the treatment with the lid, big capillary ($\varnothing_1 = 4$ mm); input voltage of 4 kV.

treated surface can help to decontaminate larger surface area using small plasma jets when reactive gas (e.g., O_2 , N_2) is added to the system, and the formation of RONS is not dependent on the mixing of plasma with ambient air. This concept may also be very beneficial for decontamination in closed areas.

3.2.1.1 | Comparison of the small and the big capillaries

The SC was specifically designed for these experiments with the intention of treating the dog's ear canal. Thus, a comparison of the BC (original design) and the SC had to take place. In Figure 8, the inhibition efficiency obtained using the small and the BC is very similar ($p = 0.97$) for the open-air treatment as well as for the treatment with the lid. This fact may be beneficial for any future adjustments of the capillary size, where an assumption of similar efficiencies can be expected. When using only helium as the plasma gas, the inhibition efficiency does not increase with the usage of the lid. This result can lead to an assumption that it is mostly the short-lived species (created mainly due to metastable helium) that are responsible for the decontamination. However, with the addition of oxygen into the system, the inhibition efficiency is highly dependent on the treatment conditions (open-air or closed area). Then, the increased inhibition efficiency with the usage of the lid can be attributed to long-lived species such as ozone, as mentioned above.

Plasma gas composition

The assumption about the strong inhibitory effects of the RONS was also supported by the experiments where different amounts of oxygen were added to the system. With an increased amount of oxygen and the usage of the

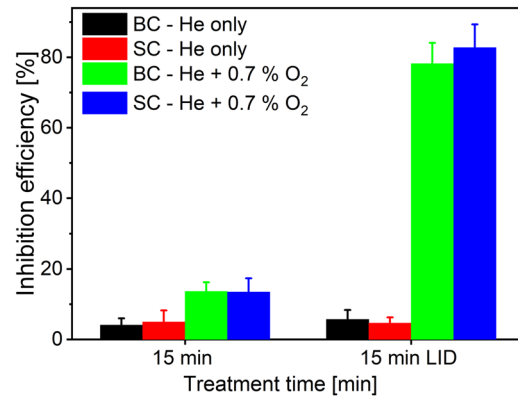


FIGURE 8 Comparison of the inhibition efficiency for the big capillary (BC, $\varnothing_1 = 4$ mm) and the small capillary (SC, $\varnothing_1 = 1$ mm) with and without oxygen admixture; input voltage of 4 kV.

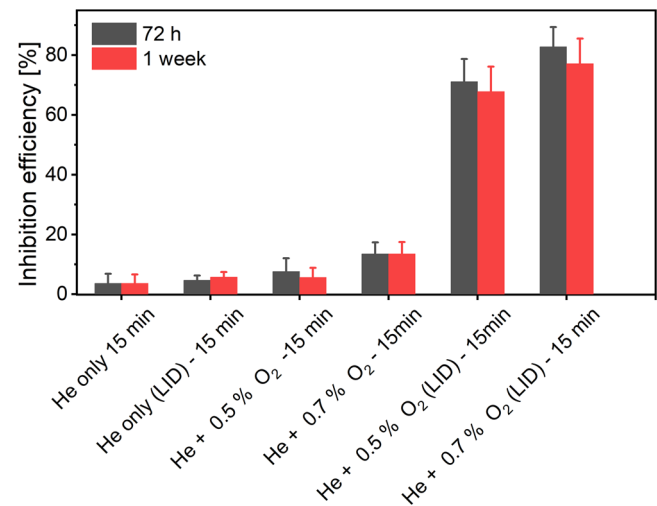


FIGURE 9 Inhibition efficiency obtained with the small capillary (SC, $\varnothing_1 = 1$ mm) by the 15-min treatment under different conditions; input voltage of 4 kV.

lid, higher inhibition efficiency was achieved (see Figure 9). The addition of reactive gas, such as oxygen or nitrogen, into the plasma gas mixture results in the formation of more active species due to the reactions taking place inside the reactor among the plasma gases themselves. Due to the energy transfers from helium excited levels or helium ions and/or direct electron impact, mainly dissociation of oxygen and excitation of nitrogen molecules occur in the capillaries and not only in the plasma plume region. Whereas in the case of using only helium, the formation of active species is highly dependent on the surrounding air that supplies oxygen and nitrogen for the formation of active species.

The time stability of the inhibited area was also examined. In all the experiments, the inhibitory effects seemed to be unchanged during the observation period

(1 week after the plasma treatment). No new colony formation was observed in the inhibited areas. A small change in the inhibition efficiency depicted in Figure 9 is caused by the growth of the cells that survived the treatment, but generally, this change was no more than 5%.

3.2.2 | RONS delivery assessment

In the KI-enriched biopolymers, iodide is oxidised to iodine by the RONS from plasma. Subsequently, the formed iodine reacts with the starch to form a complex exhibiting a dark blue colour in the visible range of the spectrum, thus turning the biopolymer colour from transparent to dark blue in places where the reaction occurred. As reported by Kawasaki et al.,^[32] this reaction can be used as a nonselective proof of RONS in the system. Altogether, the effects of hydroxyl radical (OH), atomic oxygen (O), ozone (O₃), hydrogen peroxide (H₂O₂), hydroperoxyl radical (HOO) and nitrite (NO₂⁻) can be confirmed by this agent. We were also able to approximately trace the RONS (mainly ROS in this plasma system) distribution on the treated surface for different treatment conditions and correlate them with the results obtained in the microbiological essays. It was confirmed that using only helium as the plasma gas results in the formation of a small central blue spot indicating oxidised iodine. With a small addition of oxygen into the plasma gas, the formation of RONS increases, thus leading to the enhanced inhibitory effects and formation of a bigger blue spot on the KI-enriched biopolymers. Using the lid, the whole surface of the Petri dish turns blue, mirroring the results described above (see Figure 10). It was proved that with the use of a lid, the distribution of RONS spreads over the whole area of the Petri dish compared to the treatment without the lid (the open-air treatment), where the inhibitory effects were concentrated in one spot. This also confirms the estimation that long-lived species are the main factor responsible for the large surface plasma decontamination due to their longevity, which allows them to accumulate, distribute over the surface and react with the target. With longer treatment time, bigger blue zones were formed. The amount of oxygen added to the system also influences the inhibition efficiency (as discussed above). In this proof reaction, it was observed that a darker blue colour formed after the treatment with more oxygen-rich plasma, which again contributes to the conclusion that the RONS (mainly ROS in this case) formation is the main factor responsible for microbial inactivation.

3.2.3 | Resistance of *C. glabrata* to antimycotics

The antimicrobial resistance of *C. glabrata* was evaluated after 24 h cultivation. The inhibition zones (see Figure 11) formed around the antimicrobial discs containing selected antimycotics (see Table 3) were measured. According to the evaluation sheet provided by the manufacturer, the sizes of the inhibition zones were determined to be too small for the antimycotic to be considered effective. The results prove the innate resistance of *C. glabrata* against the most commonly used azole antimycotics. Neither the antimycotics from other groups (amphotericin B, nystatin) exhibit the desired antimicrobial efficiency. We can conclude that *C. glabrata* falls into the category of intermediary or resistant to all tested antimycotics.

3.2.4 | Pork skin experiments

In these experiments, the pork skin was used as an inoculation substrate, and all the trends observed in experiments with the Petri dishes were proved, too. With longer treatment time and with the use of the lid, the inhibition efficiency was enhanced (Figure 12). Similar efficiency was achieved for the small and the big capillaries ($p = 0.82$). After the 15-min treatment with the lid, a total surface decontamination (5 log reduction) was achieved for both capillary sizes. In the open-air treatment, the microbial reduction was approximately 2–3 logs, only.

Impact of the inoculation volume and the cell concentration

Two different inoculation volumes (10 and 20 μ L) were studied to determine whether it has an impact on the antimicrobial effects of the CAP (Figure 13).

For the volume of 10 μ L, the total decontamination of the treated surface was achieved after the 10-min treatment. When the surface was infected by the volume of 20 μ L, the total decontamination was not achieved even after the 15-min treatment, but a significant microbial reduction was observed (4 logs). It may seem that with greater volume, lower inhibitory effects are achieved, but it is important to acknowledge that the number of cells inhibited by the plasma treatment was similar for both studied volumes. In both cases, the number of cells inhibited after the 10-min treatment with the lid was $\sim 10^5$ CFU/mL. Thus, we may assume that the initial cell concentration does not highly influence the inhibition efficiency, as proved in a previous experiment.^[29]

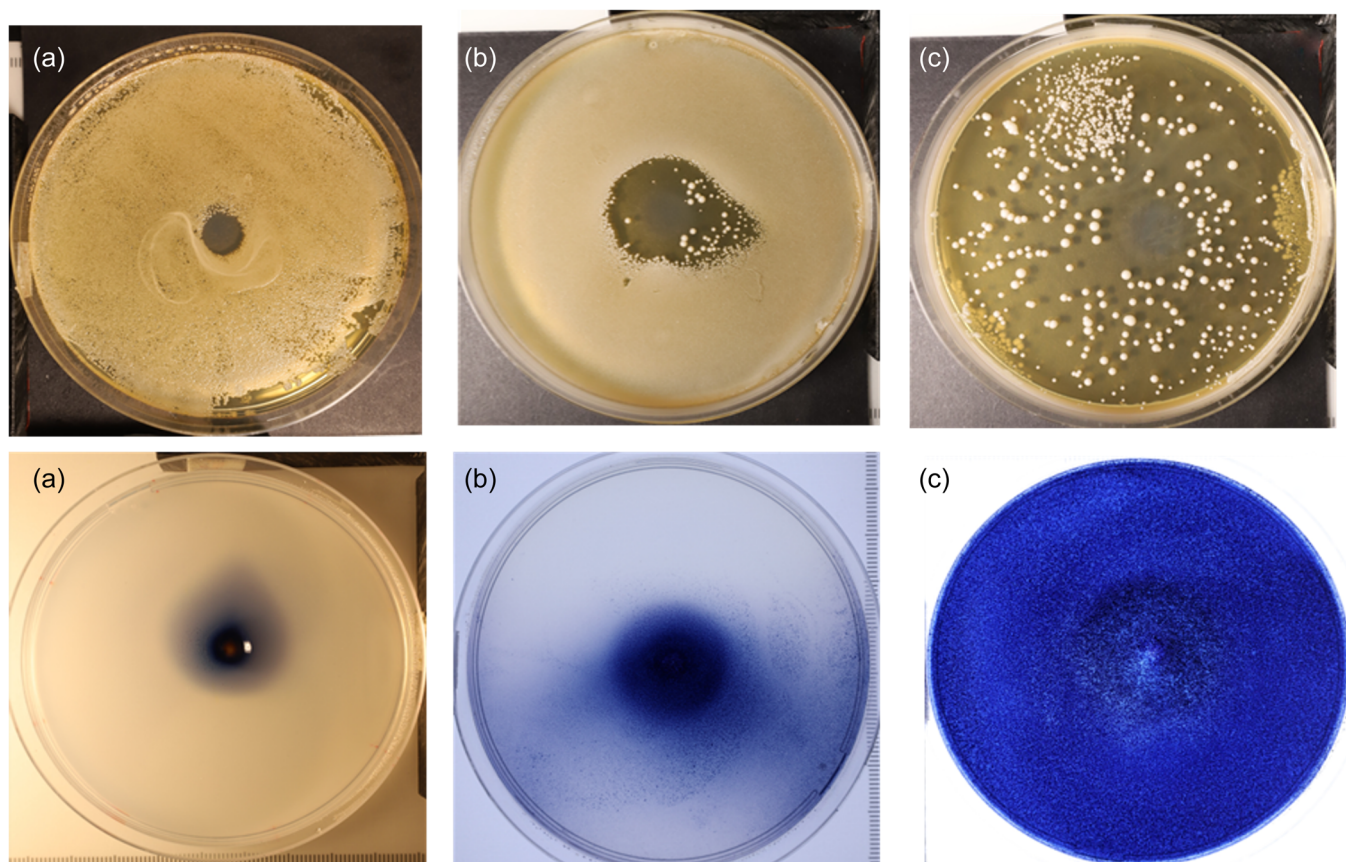


FIGURE 10 Correlation of the KI proof reactions (bottom) with the microbial assays achieved for *Candida glabrata* (up) with the small capillary ($\varnothing_1 = 1$ mm, 15 min, 4 kV), where the same treatment conditions were used for the corresponding photos in upper and bottom rows; (a) He only; (b) 0.5% O₂; and (c) 0.5% O₂ with the lid.

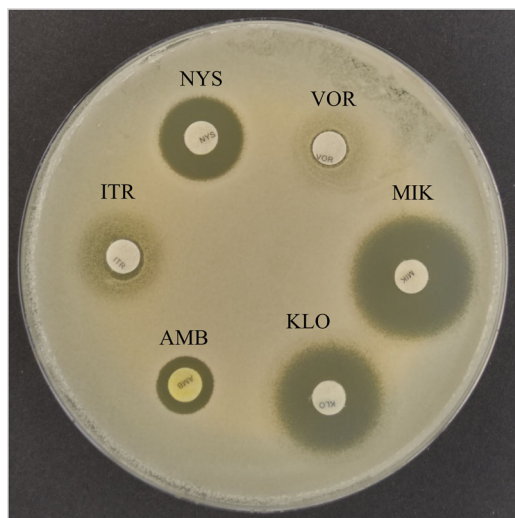


FIGURE 11 Resistance of *Candida glabrata* to selected antimycotics (acronyms are explained in Table 3).

Time stability of microbial inhibition

The time stability of the microbial inhibition was studied using the measurement of the optical density, which can be referred to as the cell concentration. In Figure 14, in

TABLE 3 Summary of results for antimycotic resistance.

Antifungal agents	Drug concentration in the disc (μg)	Susceptibility
Amphotericin B (AMB)	50	I
Itraconazole (ITR)	30	R
Nystatin (NYS)	50	I
Voriconazole (VOR)	1	R
Miconazole (MIK)	30	R
Clotrimazole (CLO)	30	R

Abbreviations: I, intermediary; R, resistant.

the nontreated control samples, the optical density increased due to the vital cell reproduction. In the case of the samples treated for 5 min in the open air, the number of cells that survived the treatment was still very high; thus, we can observe a large increase in optical density and can consider this treatment inefficient. With the use of the lid in the 5-min treatment, the number of surviving cells was much smaller, which is why the

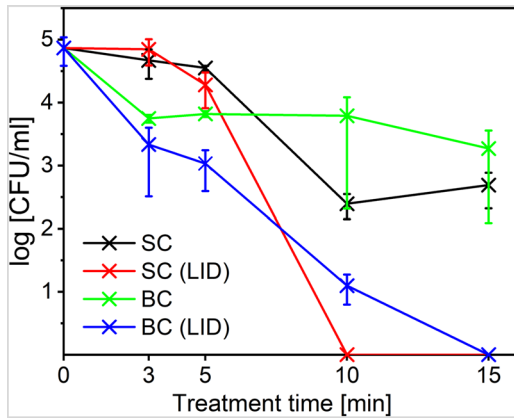


FIGURE 12 Microbial reduction achieved for the big capillary (BC, $\varnothing_i = 4$ mm) and the small capillary (SC, $\varnothing_i = 1$ mm) for different treatment times with the gas mixture (He + 0.7% O₂), where the inoculation volume for all samples was 10 μ L.

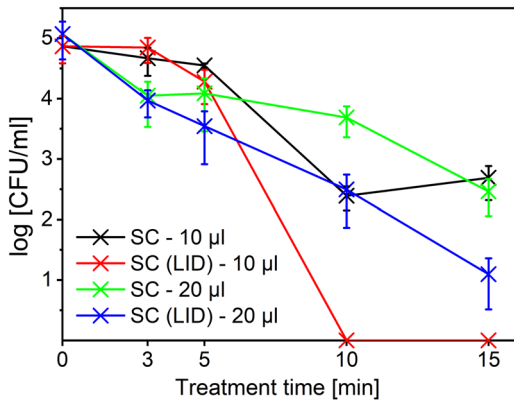


FIGURE 13 Microbial reduction achieved by the small capillary ($\varnothing_i = 1$ mm) for two different inoculation volumes and different treatment times with the gas mixture (He + 0.7% O₂).

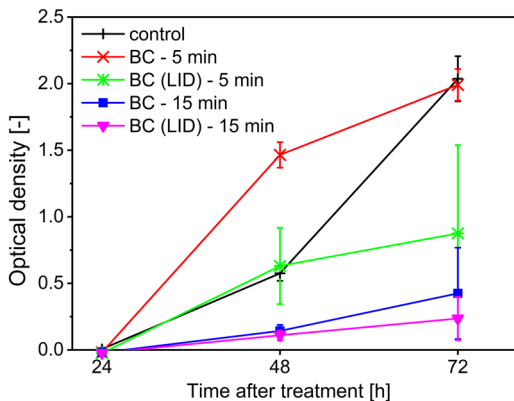


FIGURE 14 Time stability of the microbial inhibition shown for the big capillary ($\varnothing_i = 4$ mm) in different treatment times in the gas mixture (He + 0.7% O₂); inoculation volume of 50 μ L.

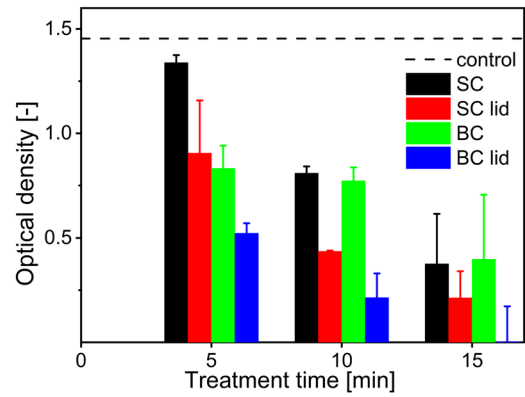


FIGURE 15 Optical density of treated samples 5 days after the plasma treatment, shown for the big (BC) ($\varnothing_i = 4$ mm) and small ($\varnothing_i = 1$ mm) capillaries (SC) in different treatment times in the gas mixture (He + 0.7% O₂); inoculation volume of 10 μ L.

optical density increased but not to the extent of the control sample. On the other hand, the optical density of the samples treated for 15 min stayed very low, which means that the number of the cells was not increasing exponentially as it would happen in healthy cells (see the control sample). Higher efficiency is again observed for the treatment with the lid. The slight increase in the optical density may be caused by the reproduction of the cells that survived the treatment. Thus, we can assume that the plasma inhibition is stable in time, and the inhibited cells are not able to repair and reproduce. Results shown in Figure 14 were evaluated for the volume of 50 μ L where the total decontamination was not achieved, which was the reason for an increase in optical density even after the 15-min treatment.

The longest-time stability was studied 5 days after the treatment. For the inoculation volume of 10 μ L, the optical density of the samples treated for 15 min with the lid stayed unchanged (at zero) even after 5 days after the treatment (see Figure 15). This result confirms the assumption that the cells that were successfully inhibited by the plasma were not able to regain their vitality and reproduce. This result does not confirm that the cells are dead, but it was observed that they are nonculturable and not able to reproduce.

3.3 | Experiments with 3D-printed models

In the experiments with the 3D-printed models of the dog ears, various types of treatments were studied. First, the surface treatment, where only the visible surface of the model was treated; second, the cavity

treatment, where only the inside (the ear canal) was treated; and lastly, the total treatment, which combined the surface and the cavity treatment. The highest inhibition efficiency was achieved for the surface treatment, while the total treatment and the cavity treatment demonstrated lower outcomes. Almost no efficiency was observed for the treatment with only helium as the plasma gas. It can be seen in Figure 16 that the inhibition efficiency of the total treatment (the surface and the cavity together) was around 30%–40%, which was in between the surface and the cavity treatment. From the statistical standpoint, this represents the significance value ($p = 0.28$) in comparison to the control samples, which is considered insignificant. However, when taking into consideration that the treatment was done on the dielectric surface (polylactic acid polymer), where substantially fewer RONS are generated (compared to the real-life conditions), the results can be considered successful. The difference in efficiency between the surface and the cavity treatment can be caused by the fact that most of the cells inside the cavity were immersed in the inoculation medium, whereas on the surface, they were only attached to the plastic polymer. Several explanations are possible, of which, one is that, ozone as the main factor responsible for the inhibition in the gas phase (as shown above) was not able to penetrate into the liquid due to its high hydrophobicity.^[33] Another reason can be that the reactive species may have been quenched in reactions with organic molecules from the medium in which the cells were immersed inside of the cavity. Despite the longevity of ozone in liquids, most molecules did not even reach the microbial cells, thus lessening the treatment efficiency. When the cells were only attached to the plastic surface, they were more susceptible to the plasma treatment because there was nothing that would prohibit the active species from reacting with the microbial cells.

The time stability of the microbial inhibition was also studied and the same effects as for the pork skin were observed. The results shown in Figure 17 are represented as an average for the different sizes of the 3D-printed models, where different initial cell concentrations were used. The optical density of the control samples highly increased 72 h after the plasma treatment, where the large standard deviations are caused by the usage of different inoculation volumes for different model ear sizes. The optical density of the samples treated for 15 min remained stable 72 h after the treatment, independent of the initial cell concentration. Thus, we may summarise that the

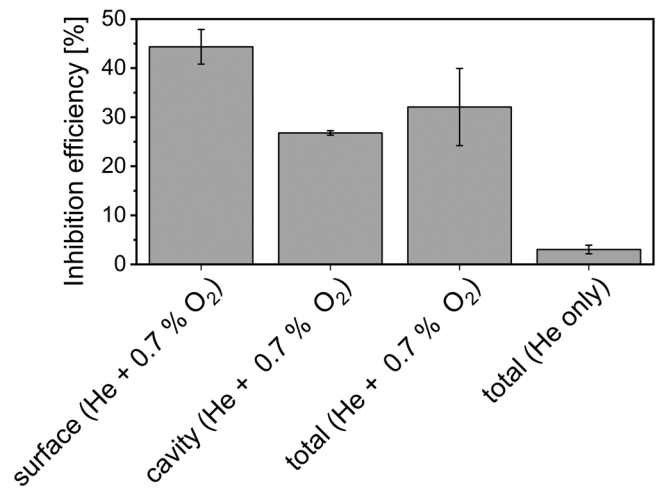


FIGURE 16 Inhibition efficiency of the different treatment types applied on the 3D-printed dog ear models (small capillary [$\phi_i = 1$ mm], $U = 4$ kV; 15 min treatment); the graph shows the average results for all dog head-sized. The first column represents the surface treatment, where only the visible surface of the model was treated; the second column depicts the cavity treatment, where only the inside (the ear canal) was treated, the third column is the total treatment (surface + cavity), and the fourth column is the total treatment with only helium plasma.

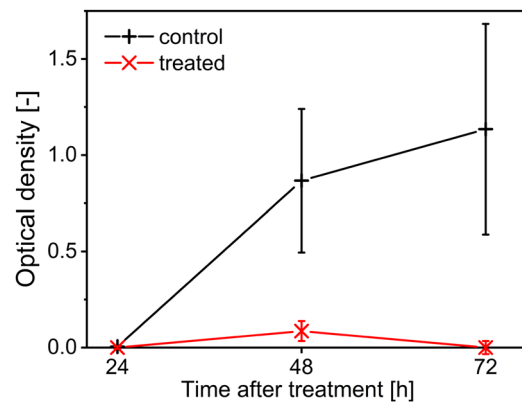


FIGURE 17 Time stability of the microbial inhibition in the 3D-printed models. Graph shows the average results for all dog head-sized.

15-min plasma treatment is efficient and stable in time for a wider range of initial cell concentrations.

4 | COMPARISON OF PLASMA GUN TO OTHER PLASMA SOURCES

To look at the results from a different perspective, it is beneficial to compare them with the results achieved previously for other plasma devices. In the recently

published articles^[29,34] about the antimycotic effects of different CAP sources tested on the same yeast strain, one cannot deny the antimycotic effects of CAP. In the case of microwave discharges, the treatment times used for successful inhibition were much shorter for the open-air treatment. This can be associated with different operating frequencies of the plasma sources (kHz for the plasma gun vs. GHz for the MW sources) and with the predominant type of RONS generated by the plasma source. In the MW discharges, the formation of active species is highly dependent on the surrounding air, and it was studied that a vast number of RONS are the RNS.^[30,35] In the case of the plasma gun, the most active species are ROS. From a biological background, it is known that some microbial species are more susceptible to RNS and others to ROS. Another difference between the MW sources and the plasma sources operating at the kHz range is the impact of the electromagnetic field. In MW sources, the electromagnetic field is in direct contact with the treated target, having an important impact, whereas in the plasma gun, the impact of the electromagnetic field is not so strong. When considering the results of bacterial assays,^[26] the treatment times used for bacterial decontamination with the plasma gun were very short (up to 1 min). We may extrapolate that these bacteria (*E. coli* and *S. aureus*) are more susceptible to ROS (especially to ozone) compared to the yeast *C. glabrata* and therefore, it takes much longer time to inactivate it. So, an assumption that the yeast *C. glabrata* is much more susceptible to RNS than to ROS arises here, which will be verified in our future experiments. The advantage of using the plasma gun is the possibility of adding oxygen or nitrogen into the plasma gas where it is possible to produce RONS independently on the surrounding air supply. This can be highly beneficial for the treatment in the enclosed areas or areas with a little air supply (like the dog ear canal) where the closure of the treated surface even helps to accumulate the RONS and to enhance the treatment efficiency.

5 | CONCLUSION

Antimycotic effects of the plasma gun were studied on three different surfaces: agar, pork skin and 3D-printed models from PLA polymer. Similar trends were observed for all studied inoculation substrates. Different parameters were evaluated and optimised to provide an effective plasma treatment for decontamination purposes. Optimisation was done with two different sizes of capillaries (big [$\varnothing_i = 4$ mm] and small [$\varnothing_i = 1$ mm]), where similar results were achieved independently on the capillary size. With the increasing treatment time, the inhibition efficiency was increased as well. For a

remarkable inhibition of *C. glabrata*, treatment times over 5 min need to be used. Therefore, a longer treatment (15-min) was studied to achieve decontamination comparable to the previously obtained results.^[26,29] Total decontamination (5–6 log) of the treated surface was achieved using the concept of the lid to cover the treated surface and enhance the RONS concentration. With the use of different inoculation volumes, it was proved that within the studied range, the plasma treatment is not highly dependent on the initial cell concentration. This means that a similar number of cells is inhibited by the plasma treatment ($\sim 10^5$ CFU/mL after the 15-min treatment). By different proof reactions (different amounts of oxygen admixture, treatment distance optimisation, KI-starch proof reactions), it was proved that the main agents standing behind the plasma decontamination are RONS produced in the plasma. The time stability of the microbial inhibition was studied up to 1 week after the treatment. It was shown that the inhibited cells stayed inhibited and were not able to repair and reproduce. It is important to note that all the experiments were done at the floating potential, where the experimental models were not grounded or placed on the metallic surface. According to previous studies,^[36,37] grounding of the treated object highly enhances the formation of RONS, leading to even higher efficiency. This means that efficiency achieved for these in-vitro measurements is only the minimum of what can be achieved in real-life treatment, where the patient (a dog or a human being) is partially conductive, has a nonnegligible capacitance and can be grounded during the treatment. We may conclude that the plasma treatment by the plasma gun can be an effective method for yeast inhibition on various surfaces as well as in closed spaces like the dog ear canals.

6 | PERSPECTIVES

As one can imagine, it is not convenient for the patient to have a stream of gas blowing to the ear for a long time. Therefore, a big perspective of this work would be to optimise the system set-up to achieve the same efficiency in a shorter treatment time with a lower gas flow. It is also important to consider the other conditions inside the dog ear canal, like the presence of cerumen, hair and other microbes that make the situation rather complex.^[38] Quantitative modelling of the effect of CAP for clinical use is, therefore, highly desirable. Further studies are planned on microbial cocultivations as well as the inclusion of other factors like standard synthetic cerumen to better simulate the real conditions.

ACKNOWLEDGEMENTS

This work was supported by the COST Action CA20114 “PlasTher” and the COST Action CA19110 “PLAgri” (supported by European Cooperation in Science and Technology) and GDR HAPPYBIO.

CONFLICT OF INTEREST STATEMENT

The authors declare no conflict of interest.

DATA AVAILABILITY STATEMENT

Data that support the findings of this study are available from the corresponding author upon reasonable request.

ORCID

Kristína Trebulová  <http://orcid.org/0000-0002-6292-4642>

REFERENCES

- [1] C. J. L. Murray, K. S. Ikuta, F. Sharara, L. Swetschinski, G. Robles Aguilar, A. Gray, C. Han, C. Bisignano, P. Rao, E. Wool, Antimicrobial Resistance Collaborators, *Lancet* **2022**, 399, 629. [https://doi.org/10.1016/S0140-6736\(21\)02724-0](https://doi.org/10.1016/S0140-6736(21)02724-0)
- [2] R. M. Rosenfeld, S. R. Schwartz, C. R. Cannon, P. S. Roland, G. R. Simon, K. A. Kumar, W. W. Huang, H. W. Haskell, P. J. Robertson, *Otolaryngol. Head Neck Surg.* **2014**, 150(1). <https://doi.org/10.1177/0194599813517083>
- [3] D. G. O'Neill, A. V. Volk, T. Soares, D. B. Church, D. C. Brodbelt, C. Pegram, *Canine Med. Genet.* **2021**, 8, 7. <https://doi.org/10.1186/s40575-021-00106-1>
- [4] A. Swinney, J. Fazakerley, N. McEwan, T. Nuttall, *Vet. Dermatol.* **2008**, 19, 373. <https://doi.org/10.1111/j.1365-3164.2008.00713.x>
- [5] D. Bugden, *Aust. Vet. J.* **2013**, 91, 43. <https://doi.org/10.1111/avj.12007>
- [6] L. S. Jacobson, *J. S. Afr. Vet. Assoc.* **2002**, 73, 162. <https://doi.org/10.4102/jsava.v73i4.581>
- [7] S. Wiegand, R. Berner, A. Schneider, E. Lundershausen, A. Dietz, *Deutsches Ärzteblatt Int.* **2019**, 91(1–2), 43. <https://doi.org/10.1111/avj.12007>
- [8] G. Kiss, S. Radványi, G. Szigeti, *J. Small Anim. Pract.* **1997**, 38, 51. <https://doi.org/10.1111/j.1748-5827.1997.tb02987.x>
- [9] L. De Martino, F. P. Nocera, K. Mallardo, S. Nizza, E. Masturzo, F. Fiorito, G. Iovane, P. Catalanotti, *Asian Pac. J. Trop. Biomed.* **2016**, 6, 384. <https://doi.org/10.1016/j.apjtb.2015.11.012>
- [10] J. Korbely, A. Singh, J. Rousseau, J. S. Weese, *Vet. Dermatol.* **2019**, 30, 228. <https://doi.org/10.1111/vde.12734>
- [11] S. J. Kim, T. H. Chung, *Sci. Rep.* **2016**, 6, 20332. <https://doi.org/10.1038/srep20332>
- [12] M. Laroussi, F. Leipold, *Int. J. Mass Spectrom.* **2004**, 233, 81. <https://doi.org/10.1088/1367-2630/11/11/115012>
- [13] M. G. Kong, G. Kroesen, G. Morfill, T. Nosenko, T. Shimizu, J. van Dijk, J. L. Zimmermann, *New J. Phys.* **2009**, 11, 115012. <https://doi.org/10.1088/1367-2630/11/11/115012>
- [14] T. Von Woedtke, A. Schmidt, S. Bekeschus, K. Wende, K. D. Weltmann, *In Vivo* **2019**, 33, 1011. <https://doi.org/10.21873/invivo.11570>
- [15] T. von Woedtke, S. Emmert, H. R. Metelmann, S. Rupf, K. D. Weltmann, *Phys. Plasmas* **2020**, 27(1). <https://doi.org/10.1063/5.0008093>
- [16] E. Robert, T. Darny, S. Dozias, S. Iseni, J. M. Pouvesle, *Phys. Plasmas* **2015**, 22(12). <https://doi.org/10.1063/1.4934655>
- [17] E. Robert, V. Sarron, D. Riès, S. Dozias, M. Vandamme, J. M. Pouvesle, *Plasma Sources Sci. Technol.* **2012**, 21, 034017. <https://doi.org/10.1088/0963-0252/21/3/034017>
- [18] E. Robert, M. Vandamme, L. Brullé, S. Lerondel, A. Le Pape, V. Sarron, D. Riès, T. Darny, S. Dozias, G. Collet, C. Kieda, J. M. Pouvesle, *Clin. Plasma Med.* **2013**, 1, 8. <https://doi.org/10.1016/j.cpme.2013.10.002>
- [19] R. Smith, A. Mastrocco, J. Prittie, J. Weltman, *Vet. Med. Res. Rep.* **2023**, 14, 125. <https://doi.org/10.2147/VMRR.S411935>
- [20] A. R. Moritz, F. C. Henriques, *Am. J. Pathol.* **1947**, 23, 695.
- [21] About Burned Skin. *BurnCentreCare: Education* **2006**. [online]. http://burncentrecare.co.uk/about_burned_skin.html
- [22] Burn Exposure Chart. *Antiscald* **2016**. [online]. https://antiscald.com/index.php?route=information/information&information_id=15
- [23] J. Hrudka. *Automatic Image Analysis of the Effects of Non-thermal Plasma on Mold Growth* [poster]. Kyoto, Japan; **2023**.
- [24] A. A. Miles, S. S. Misra, J. O. Irwin, *Epidemiol. Infect.* **1938**, 38, 732. <https://doi.org/10.1017/S002217240001158X>
- [25] Pixelbeaker Canine Ear Trainer 3D Model. *Sketchfab* **2017**.
- [26] I. Orel, F. Brulé-Morabito, A. Stancampiano, P. Escot Bocanegra, S. Dozias, J. Pouvesle, E. Robert. *Gram-Negative and Gram-Positive Bacteria Disinfection by Cold Atmospheric Plasma Using an In Vitro Agar Plate Model of a Chronic Wound* [poster]. **2022**.
- [27] T. Maho, R. Binois, F. Brulé-Morabito, M. Demasure, C. Douat, S. Dozias, P. Escot Bocanegra, I. Goard, L. Hocqueloux, C. Le Helloco, I. Orel, J. M. Pouvesle, T. Prazuck, A. Stancampiano, C. Tocaben, E. Robert, *App. Sci.* **2021**, 11, 9598. <https://doi.org/10.3390/app11209598>
- [28] K. Trebulová, F. Krčma, Z. Kozáková, P. Matoušková, *Appl. Sci.* **2020**, 10, 5538. <https://doi.org/10.3390/app10165538>
- [29] K. Trebulová, F. Krčma, P. Skoumalová, Z. Kozáková, Z. Machala, *Plasma Processes Polym.* **2023**, 20(12). <https://doi.org/10.1002/ppap.202300048>
- [30] F. Krčma, I. Tsonev, K. Smejkalová, D. Truchlá, Z. Kozáková, M. Zhekova, P. Marinova, T. Bogdanov, E. Benova, *J. Phys. D Appl. Phys.* **2018**, 51, 414001. <https://doi.org/10.1088/1361-6463/aad82b>
- [31] M. Sharma, J. B. Hudson, *Am. J. Infect. Control* **2008**, 36, 559. <https://doi.org/10.1016/j.ajic.2007.10.021>
- [32] T. Kawasaki, K. Nishida, G. Uchida, F. Mitsugi, K. Takenaka, K. Koga, Y. Setsuhara, M. Shiratani, *Jpn. J. Appl. Phys.* **2020**, 59, SHHF02. <https://doi.org/10.35848/1347-4065/ab71dc>
- [33] R. Mentheour, Z. Machala, *Front. Phys.* **2022**, 10. <https://doi.org/10.3389/fphy.2022.895813>
- [34] F. do Nascimento, A. Stancampiano, K. Trebulová, S. Dozias, J. Hrudka, F. Krčma, J. M. Pouvesle, K. G. Kostov, E. Robert, *Plasma Chem. Plasma Process.* **2023**, 43, 1791. <https://doi.org/10.1007/s11090-023-10409-9>
- [35] E. Benova, P. Marinova, R. Tafradžiiska-Hadjiolova, Z. Sabit, D. Bakalov, N. Valchev, L. Traikov, T. Hikov, I. Tsonev,

- T. Bogdanov, *Appl. Sci.* **2022**, *12*, 969. <https://doi.org/10.3390/app12030969>
- [36] Q. A. Abbas, *Iraqi J. Sci.* **2019**, *60*(6), 1251. <https://doi.org/10.24996/ij.s.2019.60.6.8>
- [37] E. Simoncelli, A. Stancampiano, M. Boselli, M. Gherardi, V. Colombo, *Plasma* **2019**, *2*, 369. <https://doi.org/10.3390/plasma2030029>
- [38] J. Sánchez-Leal, I. Mayós, J. Homedes, L. Ferrer, *Vet. Dermatol.* **2006**, *17*, 121. <https://doi.org/10.1111/j.1365-3164.2006.00504.x>

How to cite this article: K. Trebulová, I. Orel, J.-M. Pouvesle, E. Robert, A. Rouillard, A. Stancampiano, J. Hrudka, P. Menčík, Z. Kozáková, Z. Měšťánková, D. Kužmová, I. Paličková, A. Čížek, F. Krčma, *Plasma. Process. Polym.* **2024**, e2400057. <https://doi.org/10.1002/ppap.202400057>